60 GHz and 94 GHz Antenna-Coupled $LiNbO_3$ Electrooptic Modulators

Finbar T. Sheehy, William B. Bridges, and James H. Schaffner

Abstract—**Antenna-coupled $LiNbO_3$ electrooptic modulators can overcome the material dispersion which would otherwise prevent sensitive high-frequency operation. We previously demonstrated the concept with a phase modulator at *X*-band. We have extended this demonstration to a narrowband 60 GHz phase modulator, and broad-band amplitude modulator designs at 60 and 94 GHz, respectively.**

Introduction

In a previous paper [1] we reported on a prototype antenna-coupled $LiNbO_3$ electrooptic modulator at *X*-band. The antenna-coupled modulator concept was developed to overcome the material dispersion in $LiNbO_3$, which normally limits the bandwidth-sensitivity product of traveling wave $LiNbO_3$ modulators. Many short phase modulators are operated simultaneously, with the signal coupled to each one by an antenna at its input. The signal is radiated onto the array of antennas at an angle which ensures that adjacent antennas are driven with an RF signal delay equal to the optical signal delay between electrode elements. This means that there is no velocity mismatch on average. There is a mismatch in each electrode element, which limits its bandwidth, but the individual elements are kept short so that their bandwidth is sufficiently large. The bandwidth of each element is limited, however, by the coupling antenna. Other rephasing methods have been proposed by Alferness *et al.* [2], Schaffner [3], and others. These methods involve a tradeoff of bandwidth for sensitivity. As the number of electrode sections is increased, the sensitivity increases but the bandwidth about the center frequency decreases. The antenna-coupled modulator is not like this. The bandwidth of a many-section modulator is equal to that of a single-section modulator, but its sensitivity is higher. In addition, at high signal frequencies there is the practical problem of making electrical connections to the modulator without introducing unacceptable parasitics. The antenna-coupled modulator does not require physical electrical connections.

Manuscript received October 28, 1992; revised December 10, 1992. This work was supported under U.S. Air Force Contract F30602-92-C-0005 with Rome Laboratories, N. P. Bernstein, Technical Program Monitor.

F. T. Sheehy and W. B. Bridges are with the Division of Engineering and Applied Science, California Institute of Technology, Pasadena, CA 91125.

J. H. Schaffner is with Hughes Research Laboratories, Malibu, CA 90265.

IEEE Log Number 9207571.

We now report on further theoretical and experimental development of this concept. We have demonstrated a phase-modulator similar to the original prototype in design, but scaled for operation at 60 GHz. We have developed a more broad-band modulator design, and have constructed and tested prototypes at 60 and 94 GHz. The performance of these modulators was consistent with a proposed scaling law.

We present results here for both phase modulators and amplitude modulators at millimeter-wave frequencies. It is usual to measure modulator performance by specifying the voltage required for a phase-shift of π, i.e., V_π. However, we cannot measure the voltage on the electrodes. Instead, in the case of phase modulators, we measure the phase-deviation (in degrees) per $\sqrt{\text{watt}}$. The power referred to is the power-output of the klystron used as our mm-wave source. Its output power is monitored by a directional coupler and power-meter during the measurements. For a more conventional modulator, with physical electrical connections, the performance in degrees/$\sqrt{\text{watt}}$ is given by $\sqrt{2R} \times 180/V_\pi$, where R is the input impedance of the modulator. To measure the performance of an amplitude modulator we use m^2/W, the modulation index squared per watt. Again, the power is the output power of the klystron, rather than the power actually absorbed in the modulator electrodes (which is probably considerably less). For a more conventional modulator, $m^2/W = 2R\pi^2/V_\pi^2$.

Scaling Law for Antenna—Coupled Modulators

We present a scaling law for antenna-coupled modulators which can be used to predict performance when design/operating parameters are changed. The sensitivity of the modulator (measured in degrees of phase modulation per $\text{watt}^{1/2}$) scales according to the factor $L/\{\lambda \times \sqrt{N}\}$ where N is the number of antenna/electrode elements, L is the total interaction length (i.e., $L = N \times l$, where l is the length of a single element), and λ is the optical wavelength. The dependence on L and λ are common to all electrooptic phase modulators. The length l of an individual element is inversely proportional to the signal frequency, in order to ensure that the element has sufficiently large bandwidth. Hence if the interaction length L is fixed, the number of elements is proportional to the center frequency f, so the sensitivity is proportional to $\sqrt{1/f}$. Given a center frequency, the sensitivity can be

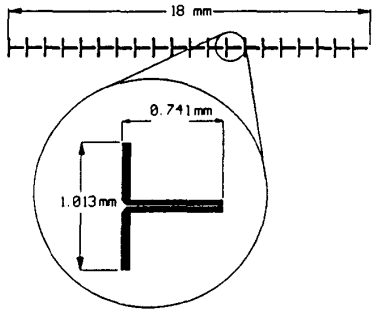

Fig. 1. Dipole antenna/electrode array used in 60 GHz antenna-coupled modulator.

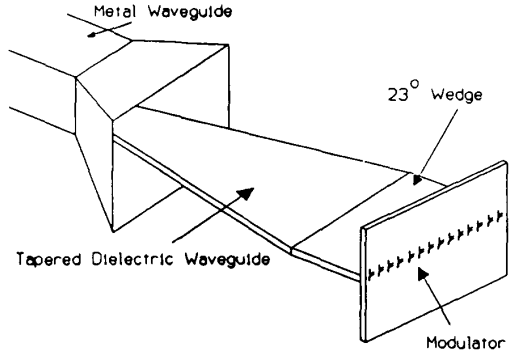

Fig. 2. RF feed structure for antenna-coupled modulators.

increased by increasing the interaction length L. However, this also involves increasing N by the same factor, so the net increase in sensitivity is proportional to $\sqrt{L}$.

Phase Modulator at 60 GHz

The 60 GHz phase modulator was based on the original X-band prototype discussed in [1], and our preliminary results were added in proof to [1]. The individual antenna/electrode elements were designed by scaling the X-band elements by a factor of 6 approximately. Since the optical waveguide does not scale, the interelectrode gap remained the same size, which in turn forced the electrode width to remain the same size also, in order to retain the same transmission line impedance. However, the electrode length and antenna length were scaled. The number of elements was increased from 5 to 20, for a shorter total interaction length of 18 mm. Fig. 1 shows this modulator.

The signal feed to the modulator had to distribute the power from the end of a V-band waveguide to the antenna array. The WR-15 waveguide dimensions are 3.76 mm × 1.88 mm, while the antenna array dimensions were 18 mm × 1 mm. The power was coupled first into a dielectric waveguide whose width tapered to reach the length of the antenna array. The power then entered a wedge-shaped $LiNbO_3$ slab waveguide through a quarter wave matching layer ($\epsilon_r = 9$). The $LiNbO_3$ wedge was cut at 23° to provide the required phase-velocity match. This wedge illuminated the antenna array through the $LiNbO_3$ modulator substrate. Fig. 2 shows the layout.

This modulator operated at 0.633 μm. As in [1], we used a scanning Fabry–Perot interferometer to measure the amplitude of the phase-modulation sidebands. Fig. 3 shows the measured response. The measurement bandwidth was limited by the tuning range of the klystron we used as a signal source. Based on subsequent experience with the 94 GHz broadband modulator measurements, we now believe that much of the structure in this frequency response may be due to an E–H tuner used in the signal feed. Unfortunately the klystron failed before we could confirm this. We can compare these results to the results previously obtained with the X-band prototype. It showed a peak sensitivity of approximately $110°/\sqrt{W}$, while the

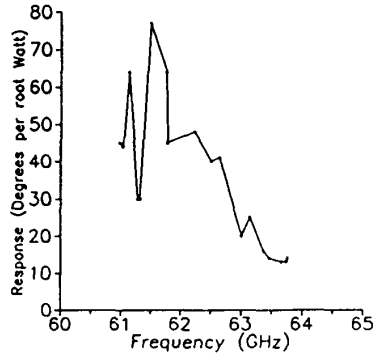

Fig. 3. Measured response of 60 GHz dipole-coupled phase modulator at 633 nm.

current modulator achieved $80°/\sqrt{W}$. This is excellent performance, as the interaction length has been reduced and the operating frequency increased. Based on the scaling law we would have expected a sensitivity of approximately $40°/\sqrt{W}$ at 60 GHz. The higher sensitivity suggests that the 60 GHz modulator is coupled to the input signal more efficiently than was the X-band prototype. Since the other millimeter-wave modulators have essentially the same RF feed as the new modulator, we will use it as a basis for comparison.

Broad-Band Modulator at 60 GHz

The prototype modulator, and the 60 GHz modulator based on it, were narrow-band designs. The antennas used were dipoles, and the modulator electrodes were unterminated. The impedances and lengths were chosen so that the antenna-electrode combination was resonant at the design frequency. We then designed a broad-band modulator using bowtie antennas, which have nearly constant impedance over a large bandwidth [4], [5]. This type of antenna is relatively insensitive to connections made to the ends of the antenna arms, so we made provision for dc bias connections. These are necessary if the modulator is to be a Mach–Zehnder amplitude modulator, as such a modulator must be biased to its proper operating point. Two versions of this design were produced, one designed

to operate at 60 GHz, the other at 94 GHz. The optical waveguides were designed for 1.3 μm operation rather than 0.633 μm as before.

A 60 GHz integrated Mach–Zehnder amplitude modulator was prepared, based on this new design (Fig. 4). The modulator electrodes were designed to phase modulate one arm of the modulator, while the other arm would be unmodulated. The optical waveguides were sized for operation at 1.3 μm; however, the modulator was ready before a 1.3 μm laser became available, so initial testing was done with a He–Ne laser at 0.633 μm. Due to the overmoded optical waveguides the Mach–Zehnder modulator could not be operated as an amplitude modulator, but could be operated as a phase modulator by setting the dc bias so that the output was a maximum. The phase modulation of the output was then half that produced by the modulator, due to the presence of unmodulated light from the other arm of the interferometer. The results could thus be corrected to compute the phase modulation produced by the modulator itself. This experiment was performed, with the results shown in Fig. 5. Unfortunately, due to the untimely failure of the klystron, we were unable to remeasure this modulator at 1.3 μm as intended. We used an *E–H* tuner here as well, which may account for some of the structure in the frequency response.

The broad-band antennas were expected to reduce the response by a factor of 2 compared to the dipole antennas, and the interaction length was reduced from 18 mm to 12 mm, resulting in an expected response of approximately $30°/\sqrt{W}$. The measured peak response of $26°/\sqrt{W}$ is consistent with this.

Broad-Band 94 GHz Modulator

The 94 GHz modulator was based on the same design as the broadband 60 GHz modulator shown in Fig. 4. However, there were now 25 antennas covering a 12 mm interaction length. With reference to Fig. 4, the dimensions shown as 1.08 mm and 0.625 mm were reduced to 0.69 mm and 0.40 mm respectively. The feed system was very similar, except that the signal originated in a WR-10 metal waveguide, and the quarter-wave matching layer thickness was changed. In addition, by this time a 1.3 μm laser was available to test the modulator. Compared to the 60 GHz narrowband phase modulator's performance (with dipoles) at 0.633 μm, we expected to see reduced performance due to the longer optical wavelength, shorter interaction length (12 mm), increased number of antennas, and use of broad-band (nonresonant) antennas. The scaled value for a single-arm response was $12°/\sqrt{W}$. Since this modulator is a Mach–Zehnder amplitude modulator, this corresponds to a modulation index squared per watt (m^2/W) of 0.044.

The measured response is shown in Fig. 6. There is a gap in the curve because of the 8 GHz FSR of the scanning Fabry–Perot used to measure the sidebands. Since 96 is a multiple of 8, the aliases of the carrier fall on top of the sidebands at 96 GHz. The response of the

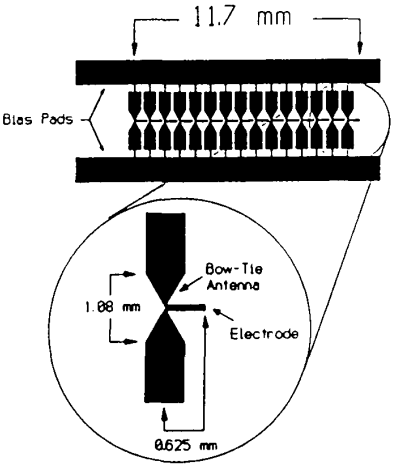

Fig. 4. Bowtie antenna/electrode array used in broad-band 60 GHz Mach–Zehnder modulator.

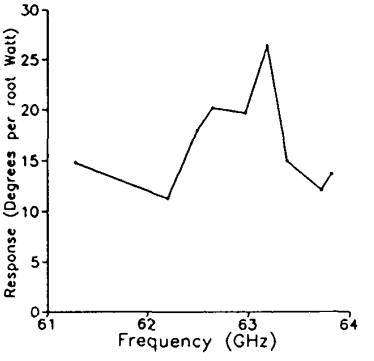

Fig. 5. Measured response of modulated arm of broad-band 60 GHz Mach–Zehnder modulator at 633 nm, as deduced from a Fabry–Perot measurement of phase modulation.

modulator is approximately $m^2/W = 0.055$ over the measured range, corresponding to single-arm phase modulation of $13°/\sqrt{W}$. This is consistent with the result expected from applying the scaling law to the performance of the 60 GHz phase modulator. The modulator does have a peak response of $m^2/W = 0.072$, corresponding to single-arm modulation of $15°/\sqrt{W}$, which is somewhat higher than expected. The frequency range of the measurement was again limited by the tuning range of the klystron, so we can only say the bandwidth is greater than 7 GHz. Lacking a photodetector with response at 100 GHz, we have, of course, no direct measurement of amplitude modulation.

Summary

We have demonstrated sensitive antenna-coupled integrated $LiNbO_3$ electrooptic modulators at 61–63 GHz and at 91–98 GHz. We have tested narrow- and broad-band designs. The measured results are consistent with the proposed scaling law for antenna-coupled modulators. Sensitivity can be increased by increasing the number of

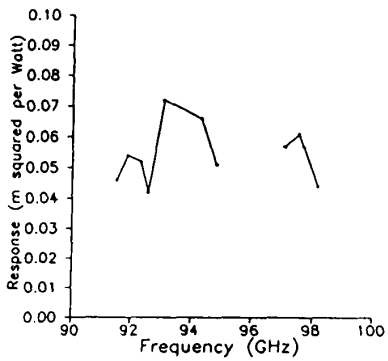

Fig. 6. Measured response of 94 GHz Mach–Zehnder modulator at 1.3 μm.

elements to obtain greater length, and by improving the slab waveguide illumination scheme. These can be done without affecting the bandwidth, which remains equal to the bandwidth of a single antenna/electrode element.

ACKNOWLEDGMENT

The authors wish to acknowledge the technical support of R. E. Johnson and R. L. Joyce, and helpful discussions with N. P. Bernstein and B. M. Hendrickson.

REFERENCES

[1] W. B. Bridges, F. T. Sheehy, and J. H. Schaffner, "Wave-coupled $LiNbO_3$ electrooptic modulator for microwave and millimeter-wave modulation," *IEEE Photon. Technol. Lett.*, vol. 3, pp. 133–135, Feb. 1991.

[2] R. C. Alferness, S. K. Korotky, and E. A. J. Marcatili, "Velocity-matching techniques for integrated optic traveling wave switch modulators," *IEEE J. Quantum Electron.*, vol. QE-20, pp. 301–309, Mar. 1984.

[3] J. H. Schaffner, "Analysis of a millimeter wave integrated electro-optic modulator with a periodic electrode," in *Proc. SPIE OE-LASE Conf. 1217*, Los Angeles, CA, Jan. 16–17, 1990, pp. 101–110, paper 13.

[4] D. B. Rutledge and M. S. Muha, "Imaging antenna arrays," *IEEE Trans. Antenn. Prop.*, vol. AP-30, pp. 535–540, July 1982.

[5] R. C. Compton, R. C. McPhedran, Z. Popovic, G. M. Rebeiz, P. P. Tong, and D. B. Rutledge, "Bow-tie antennas on a dielectric half-space: theory and experiment," *IEEE Trans. Antenn. Prop.*, vol. 35, pp. 622–631, June 1987.

Polarization-Independent Field-Induced Absorption-Coefficient Variation Spectrum in an InGaAs/InP Tensile-Strained Quantum Well

K. G. Ravikumar, T. Aizawa, and R. Yamauchi

Abstract—**We report the absorption-coefficient variation of a tensile-strained InGaAs / InP quantum well measured throughout the spectral range near and away from the band gap. We discuss the spectral absorption-coefficient variation spectra of an unstrained, a 0.15%, a 0.30% a 0.45% tensile-strained quantum well and show that the difference between the wavelengths of absorption-coefficient variation peak for TE and TM modes becomes zero with 0.3% tensile strain. We will also show that this wavelength difference varies linearly with the magnitude of the strain.**

INTRODUCTION

THE quantum-confined Stark effect (QCSE) [1], i.e., the field-induced absorption/index variation in QW structures, has been widely used for high-speed, monolithically integrable semiconductor optical switches and modulators. This spectral absorption/index variation has different profiles for TE and TM modes [2], [3] of the incident light. For example, at a wavelength where the absorption/index variation is a maximum on the negative side, for the TE mode, it becomes positive for the TM mode. To overcome this problem, we have proposed a tensile-strained quantum well [4] and reported on the observation of polarization-independent absorption variation at wavelengths longer than the bandgap wavelength [5]. Some theoretical studies [7] and waveguide interferometric switches based on this effect were also reported [6]. Until now, to our knowledge, no investigation has been reported on the polarization-independent QCSE near the bandgap, where the excitonic effect is stronger.

In this letter we report on the electric-field-induced absorption variation spectra in an unstrained, a 0.15%, a 0.30%, a 0.45% tensile-strained InGaAs quantum well

Manuscript received October 19, 1992.

The authors are with the Optical Device Section, Advanced Tech. R & D Center, Chiba 285. Japan.

IEEE Log Number 9207565.